Electron-Transfer Reactions with Significant Changes in Structure. Unsymmetrical Crowded Ethylenes

Norma A. Macías-Ruvalcaba and Dennis H. Evans*

Department of Chemistry, University of Arizona, Tucson, Arizona 85721

Received: August 30, 2006; In Final Form: September 23, 2006

The electrochemical reduction mechanisms of xanthylideneanthrone, **6**, thioxanthylideneanthrone, **7**, 10-(diphenylmethylene)anthrone, **8**, and 9-(diphenylmethylene)-9*H*-fluorene, **9**, have been studied in dimethylformamide. The reduction of the first two compounds proceeds from folded forms of the neutral to twisted forms of the anion radical according to a square scheme. The data for reduction of **8** can be well accounted for by the same square scheme. However, one-step reduction with concerted electron transfer and structural change cannot be ruled out. Compound **9**, whose fluorene ring system cannot fold, exists only in twisted forms in the neutral, anion radical, and dianion. Consequently, there are no major changes in structure upon reduction, and the compound is reduced in two reversible steps with the second complicated by rapid loss of the dianion that is probably due to protonation by components of the medium.

1. Introduction

There are many examples of molecules that undergo significant structural change upon oxidation or reduction. Examples include such symmetrical-crowded molecules as bianthrone, **1**,[1] (reduction and oxidation), bis(dimethylamino)arenes, (e.g., **2)**,[2] (oxidation), analogues of tetrathiafulvalene, (e.g., **3)**,[3] (oxidation), dinitroarenes, (e.g., **4)**,[4] (reduction), analogues of tetracyanoquinodimethane (e.g., **5**),[5] (reduction), *trans*-2,3-dimethyl-2,3-dinitrobutene,[6] (reduction), some 1,4-dialkylamino-1,3-butadienes[7] (oxidation), and others. In many cases, these structural changes, driven by steric forces, bring about an inversion in standard potentials. That is, for a reduction, the potential for insertion of the second electron, E°_2, is more positive than that for the first, E°_1, meaning that the second reduction occurs more readily than the first, $E^\circ_1 - E^\circ_2$ being negative. Numerous examples of this behavior have been reported and references may be found in ref 5.

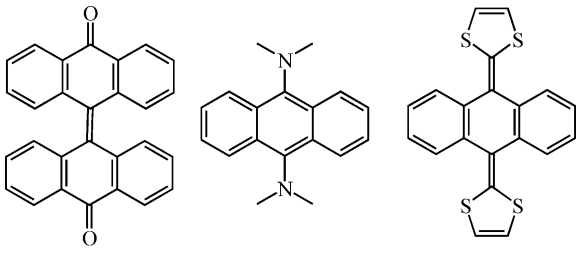

As noted above, these species are symmetrical, and they feature an overall two-electron reduction with a formal potential, $E^\circ_{overall} = (E^\circ_1 + E^\circ_2)/2$. Thus, the reaction mechanism inherently involves two electrons. However, in the molecules investigated in this study, their unsymmetrical structures allow the introduction of the first electron to occur prior to introduction of the second (see **6**−**9**). For example, in **6,** the anthrone unit is easily reduced, but the xanthylidene group is more difficult to reduce. Thus, we should be able to study the structural changes associated with the first electron transfer without interference from the second. The same holds for **7** and **8,** but in **9** no significant structural change takes place, and we find that introduction of the two electrons occurs at very negative potentials with a value of $E^\circ_1 - E^\circ_2 = 0.35$ V. In this investigation, we show that the first step of reduction of **6**−**8** is accompanied by significant structural change, that this is most likely a two-step reaction (electron transfer followed by structural change) for **8**, and that this is most certainly the case for **6** and **7**.

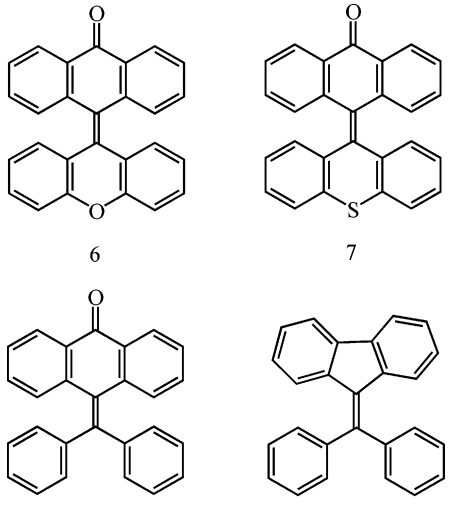

* To whom correspondence should be addressed. E-mail: dhevans@email.arizona.edu.

10.1021/jp065634s CCC: $33.50
Published on Web 11/09/2006

2. Experimental Section

2.1. Chemicals and Reagents. The solvent was *N*,*N*-dimethylformamide (DMF) and the electrolyte was tetrabutylammonium hexafluorophosphate (Bu_4NPF_6). Sources and treatment of solvent and electrolyte previously have been described.[8] The compounds 10-(9*H*-xanthen-9-ylidene)-9(10*H*)-anthracenone, or xanthylideneanthrone, **6**, and 10-(9*H*-thioxanthen-9-ylidene)-9(10*H*)-anthracenone, or thioxanthylideneanthrone, **7**, were prepared according to the method described by Schönberg, et al.[9] and purified by several successive recrystallizations from acetic acid, 1,1,2,2-tetrachloroethane, benzene, and dichloromethane. Purity and identity of the compounds was confirmed by melting point (**6**, mp 308 °C, lit. 308 °C;[9] **7**, mp 323 °C), and for compound **7**, by high-resolution mass spectrometry (M^+, 388.1032 (obsd); 388.0922 (theor)). The compound 10-(diphenylmethylene)-9-anthracenone, or 10-(diphenylmethylene)anthrone, **8**, was prepared according to the method described by Padova[10a] and purified by successive recrystalizations from acetic acid and ethanol (mp 210−211 °C, lit. 195−197 °C,[10a] lit. 205−207 °C[10b]).

The compound 9-(diphenylmethylene)-9*H*-fluorene, **9**, was obtained from Alfa Aesar and was used as received.

2.2. Electrochemical Cells, Electrodes, and Instrumentation. All of this equipment was described earlier.[8] Specifically, the working electrode was a 0.3-cm diameter glassy carbon electrode whose area was determined to be 0.0814 cm^2. The reference electrode was a silver wire immersed in 0.10 M Bu_4NPF_6/0.010 M $AgNO_3$ in acetonitrile. The potential of this reference electrode was periodically measured with respect to the reversible ferrocene/ferrocenium potential, and all potentials reported in this work are with respect to ferrocene. The temperature of the jacketed cell was controlled with a circulating bath. The reference electrode was at room temperature (nonisothermal operation). Voltammograms with only solvent and supporting electrolyte were recorded and subtracted from the voltammograms of the compounds to obtain background-corrected data. All voltammetric experiments were conducted in DMF containing 0.10 M Bu_4NPF_6.

Variation of the scan rate, υ, was done in such a way that there was an approximately linear variation in log υ. Thus for scan rates between 0.1 and 30 V/s, the values chosen were 0.1, 0.2, 0.3, 0.5, 1, 2, 3, 5, 10, 20, and 30 V/s (log $\upsilon = -1$, -0.699, -0.523, -0.301, 0, 0.301, 0.477, 0.699, 1, 1.301, 1.477).

2.3. Determination of the Equilibrium Constant for Conversion of the A to B Forms of 6. Measurements were performed with a Spectral Instruments, Inc., charge-coupled device (CCD) array UV−vis spectrophotometer equipped with a fiber-optic dip cell with a path length of 1.03 ± 0.03 cm. The absorption measurements were made at the λ_{max} of the B form, 755 nm, in spectroquality DMF (Fluka) at temperatures from 25 to 82 °C. The absorbances were converted to concentrations of B using the molar absorptivity reported by Kortüm and Zoller,[11] 1.03×10^4 M^{-1} cm^{-1} measured in cyclohexyl acetate. The initial concentration of **6** was 3.1×10^{-3} M.

2.4. Calculations. Digital simulations were conducted with DigiElch, version 2.0, a free software package for the digital simulation of common electrochemical experiments (http://www.digielch.de).[12] The fitting routine in that program was used to establish the final best-fit parameter values for many of the variables.

Complete geometry optimization and frequency calculations were performed according to the density functional theory (DFT) using the B3LYP/6-31G(d,p) level with the Gaussian 03 program.[13] For each structure, it was confirmed that there were no imaginary frequencies. For radicals, the corresponding unrestricted (UB3LYP) method was used.

3. Results and Discussion

3.1 Expected Structures of the Neutral and Anion Radical Forms of 6−9. There are two general structures associated with these compounds. The first, designated A, shows little or no twisting about the ethylenic bond, while in the second, B, there is a considerable degree of twisting. There are other important structural features. In compounds **6**−**8**, the A form features a folding of the anthrone ring system so as to reduce steric interactions with the substituent in its 10 position. In the twisted B versions, the anthrone group is almost planar. The colored B form is generally of higher energy than the A form and is thermally accessible for **6** and **8** (i.e., these compounds are thermochromic). Compound **7** is not thermochromic, which is probably because of the larger energy difference between A and B (see below).

In the anion radicals, the double-bond character of the ethylene is diminished making it easier to reduce steric interactions by twisting. In fact, the anion radical, $B^{\bullet-}$, is of lower energy than $A^{\bullet-}$ for **6** and **7** indicating that the reduction is likely to proceed at room temperature by the sequence A → $A^{\bullet-}$ → $B^{\bullet-}$. The four structures calculated for the neutral and anion radical of **6** are shown in Scheme 1. Very similar structures are found for **7**. For **8**, however, only a folded form of the neutral (A) and only a twisted form of the anion radical ($B^{\bullet-}$) could be found. These structures are shown in Scheme 2, and various energies and structural parameters are summarized in Table 1 together with relevant values from the literature.

The calculations show a free energy change of 2.1 kcal/mol for neutral **6** going from the A to the B forms. This is consistent with an experimental change in enthalpy of 3.5 kcal/mol,[14] our own determination of the enthalpy change of 3.0 kcal/mol, and an earlier calculated energy difference of 2.6 kcal/mol.[15] Our calculated free energy change for neutral **7**, 9.2 kcal/mol, is much larger than that for **6**, consistent with the fact that **7** is not thermochromic (i.e., the population of the colored B form of **7** is insignificant at all accessible temperatures).

It is costly in energy to twist the central ethylene bond when going from neutral A to B (see twist angles and $\Delta G°_{298}$ in Table 1). This is partially offset by the favorable planarization of the anthrone and xanthylidene (thioxanthylidene) ring systems. The fact that the free energy difference for **7** is larger than for **6** is probably because of the doubly folded A form being less unfavorable for **7**. The folding of the thioxanthylidene unit is facilitated by its preferred smaller C−S−C bond angle (97.6°) compared to the C−O−C angle in **6** (115°).[18] The greater degree of folding results in a larger bowsprit angle at S (32.6°) than at O (27.2°; all data in Table 1).

The twisted forms of the anion radicals, $B^{\bullet-}$, are favored over the folded forms, $A^{\bullet-}$, with the calculated free energy differences being −17.2 for **6** and −11.0 kcal/mol for **7**. This is accompanied by a lengthening of the ethylene bond in **6** from 1.370 to 1.474 Å (neutral A to anion radical B) and 1.366 to 1.484 Å for **7**, in accord with loss of double-bond character upon reduction.

Compound **8** is thermochromic but the existence of a high-temperature B form was strongly doubted in the early literature.[10b,19] Indeed, we were unable to locate such a form by calculation, which of course does not prove that it does not exist. By contrast, the anion radical of **8** is, by calculation, a strongly twisted B-type species, twist angle of 54.1° (90° by electron paramagnetic resonance (EPR)[16]).

SCHEME 1: Optimized Structures of Xanthylideneanthrone, 6, for the Two Minimum Energy Structures Found for the Neutral, A (a) and B (b), and for the Anion Radical, $A^{\bullet-}$ (c) and $B^{\bullet-}$ (d).

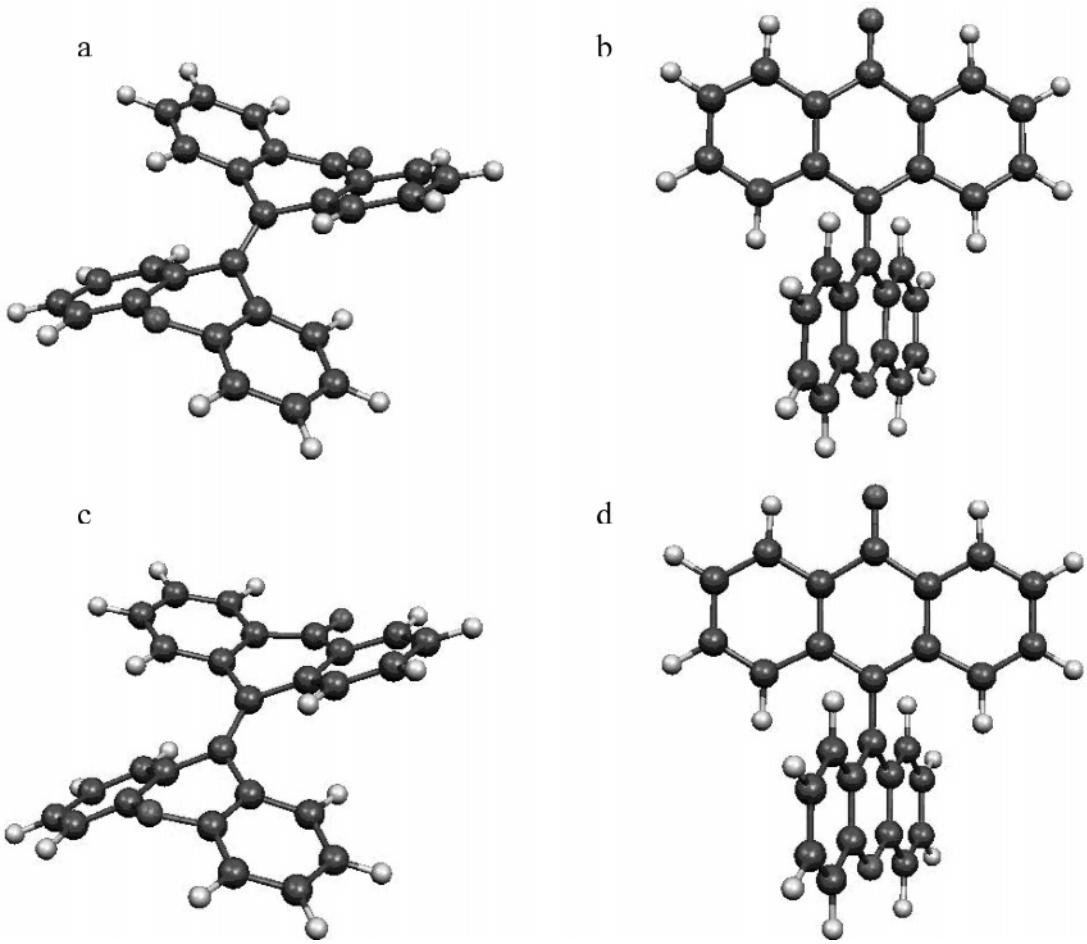

SCHEME 2: Optimized Structures of Neutral (a) and Anion Radical (b) of 10-(diphenylmethylene)Anthrone, 8.

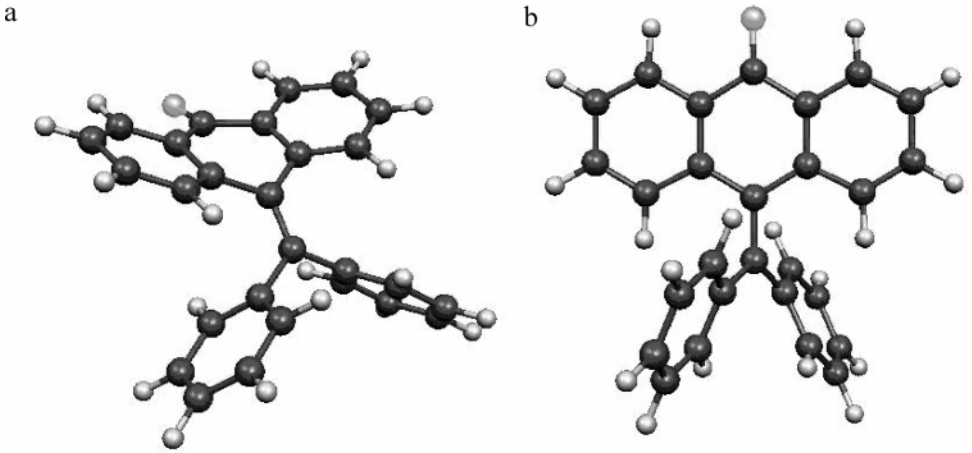

For compound **9**, folding of the fluorenyl unit is not possible. All three oxidation states (neutral, anion radical, and dianion) are calculated to be twisted with the degree of twisting increasing in that order (Table 1).

As the equilibrium constant for the conversion of neutral A to B for **6** turned out to be of great importance in the interpretation of the voltammetric behavior of this compound, we determined this constant in DMF as a function of temperature using the method described in the Experimental Section, which relies on the molar absorptivity of the B form reported by Kortüm and Zoller.[11] The results are shown in Figure 1 from which the least squares line, $\ln K_{A\rightleftharpoons B} = -1530(1/T) - 0.21$, is derived. The slope of this line gives $\Delta H° = 3.0$ kcal/mol compared to 3.5 kcal/mol reported earlier (dimethyl phthalate solvent).[14]

3.2 Voltammetric Study of 6. Voltammograms obtained at a relatively large scan rate of 20 V/s are shown in Figure 2. Assignment of the processes responsible for each peak is indicated in Figure 2. The A form is dominant at 25 °C (99.5 % present as A) so the first reduction peak is assigned to the reaction $A + e^- \rightleftharpoons A^{\bullet-}$. Reversal of the scan just past this peak reveals no peak for $A^{\bullet-} \rightleftharpoons A + e^-$, indicating that the reaction

TABLE 1: Calculated Structural Parameters and Energies of the Neutral and Anion Radicals of 6−9 and Comparison with Literature Values[a]

compound	oxidation state/structural form	dihedral angle ("twist angle")/°	bowsprit angle (anthrone)/°	$\Delta G°_{298}$/kcal mol^{-1} (A form to B form)	ethylene bond length/Å	C−O−C or C−S−C angle/°	bowsprit angle (O or S)/°
6	neutral, A	3.1	33.9	2.1 (3.5)[b] (3.2)[c] (2.6)[d]	1.370	115.0	27.2
	neutral, B	53.1 (53.3)[d]	0 (planar)		1.423	119.8	0 (planar)
	anion radical, A	3.7	27.7	−17.2	1.413	113.1	32.6
	anion radical, B	66.1 (90)[e]	0 (planar)		1.474	119.7	0 (planar)
7	neutral, A	1.9	32.3	9.2	1.366	97.6	32.5
	neutral, B	57.0	0 (planar)		1.434	103.5	0 (planar)
	anion radical, A	6.3	26.5	−11.0	1.413	96.6	36.9
	anion radical, B	71.3	0 (planar)		1.484	103.8	0 (planar)
8	neutral, A	10.1	29.4	na[f]	1.367	na	na
	anion radical, B	54.1 (90)[e]	0 (planar)	na[f]	1.463	na	na
9	neutral, B	12.7	na	na[h]	1.340	na	na
	anion radical, B	38.3 (25)[g]	na	na[h]	1.436	na	na
	dianion, B	67.2	na	na[h]	1.495	na	na

[a] Dihedral angle is between the anthrone unit (fluorene in **9**) and the 10-substituent. Bowsprit angle (anthrone) is between the 10-substituent and the boatlike central ring in the anthrone unit of **6**−**8**. Bowsprit angle (O or S) is between the O atom in xanthylidene (S atom in thioxanthylidene) and the boatlike central ring in **6** and **7**. See illustration:

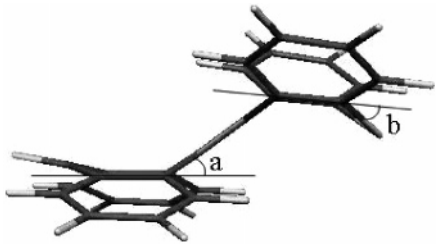

[b] DH° in dimethyl phthalate (ref 14). [c] In DMF (this work). [d] ΔE (DFT calculations using B3LYP 6-31G* from ref 15). [e] Determined by EPR in tetrahydrofuran (THF) solutions (ref 16). [f] Only one form found: folded for the neutral (A) and twisted for the anion radical ($B^{\bullet-}$). [g] By EPR (ref 17). [h] Only twisted forms found (B-forms).

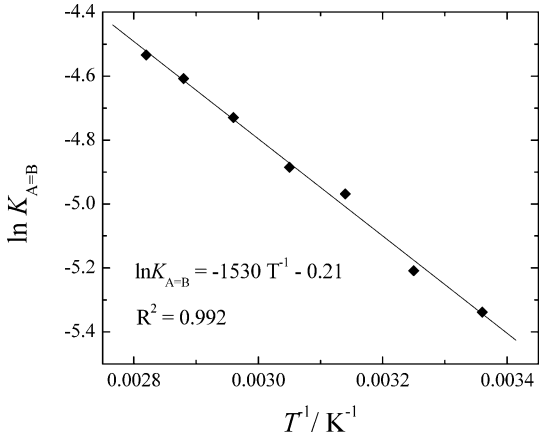

Figure 1. Temperature dependence of the equilibrium constant for A ⇌ B, $K_{A⇌B}$, for xanthylideneanthrone, **6**.

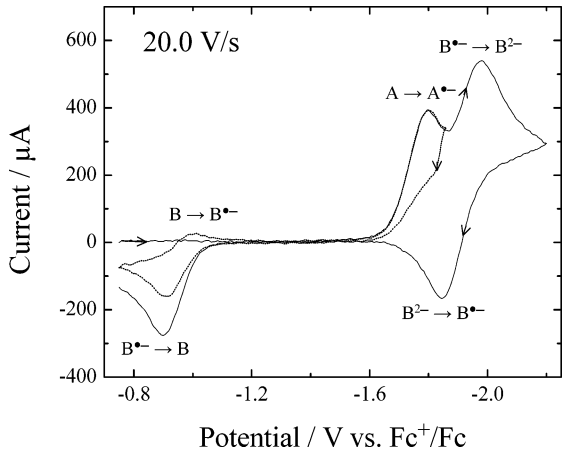

Figure 2. Background-corrected experimental voltammograms of 2.12 mM xanthylideneanthrone, **6**. Temperature: 25 °C.

$A^{\bullet-} \rightleftharpoons B^{\bullet-}$ is quite fast. In fact, no peak for oxidation of $A^{\bullet-}$ is seen at scan rates as large as 100 V/s and temperatures as low as ca. −60 °C.

When the scan is continued in the negative direction past the first peak, a second reduction peak appears, which is due to the reduction of $B^{\bullet-}$ formed at the first peak. This process is reversible with a large peak appearing for oxidation of B^{2-}. At lower scan rates, some B^{2-} is lost, and a small peak appears near −0.7 V (not shown), which may be due to a product formed by protonation of strongly basic B^{2-} by some component of the medium, trace water, for example.

Upon scan reversal after either the first or second peak, a peak for oxidation of $B^{\bullet-}$ to B is seen near −0.95 V. This process is reversible as indicated by the second reductive scan that reveals a small peak for $B + e^- \rightleftharpoons B^{\bullet-}$. This means that the rate of conversion of the high temperature B form to the favored A form is sufficiently slow so that it can be evaluated by voltammetry.

As will be seen in our fits of simulations to the experimental voltammograms, the difference in the standard potentials for the two steps of reduction of B, $E°_{1B}$ and $E°_{2B}$, is 0.83 V, which is a rather large splitting for successive steps of reduction of a compound. For example, the difference in potentials for the two steps of reduction of the B form of bianthrone, **1**, is only 0.30 V.[1] However, bianthrone is symmetrical and contains two identical reducible anthrone units. Compound **6**, on the other hand, is unsymmetrical. The anthrone unit is the more easily reduced moiety, and the introduction of the second electron is much more difficult to achieve.

Not visible in the voltammograms of Figure 2 is a small amount of current on the first negative-going sweep in the region

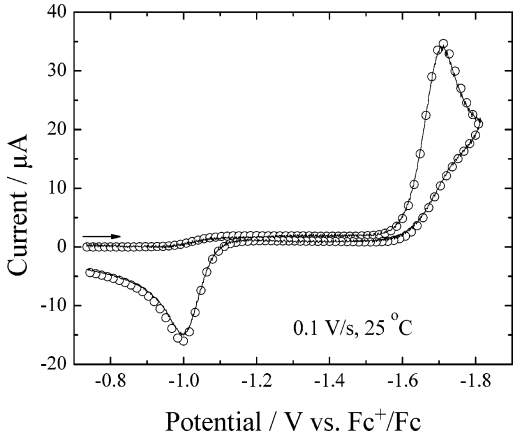

Figure 3. Voltammogram (solid curve) of 2.40 mM xanthylideneanthrone, **6**. Symbols: simulation using the parameter values listed in Table 2.

SCHEME 3

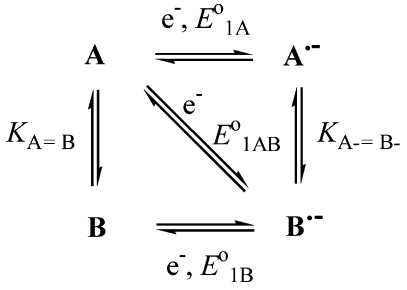

from −1.0 V to the foot of the first reduction peak. At lower scan rates at 25 °C, this current is quite apparent, and it forms a plateau which is suggestive of chemical reaction preceding the electrochemical reduction of B (a mechanism involving a Chemical reaction followed by an Electrochemical reaction, or CE mechanism) (Figure 3). That chemical reaction is presumed to be the conversion of A to B, the unfavorable structure at this temperature. It is important to note that the contribution from the reduction of the equilibrium concentration of B (∼0.5%) is negligible. Instead, the current is almost entirely kinetic in character.

The simulated curve in Figure 3 corresponds to the square Scheme 3.

Thermodynamic and kinetic parameters are associated with each reaction in the scheme are given with reactions 1−4.

$$A \rightleftharpoons B \; K_{A\rightleftharpoons B}, \qquad k_{A\to B}, k_{B\to A} \tag{1}$$

$$B + e^- \rightleftharpoons B^{\bullet -} \; E^\circ_{1B}, \qquad k_{s,1B}, \alpha_{1B} \tag{2}$$

$$A + e^- \rightleftharpoons A^{\bullet -} \; E^\circ_{1A}, \qquad k_{s,1A}, \alpha_{1A} \tag{3}$$

$$A^{\bullet -} \rightleftharpoons B^{\bullet -} \; K_{A-\rightleftharpoons B-}, \qquad k_{A-\to B-}, k_{B-\to A-} \tag{4}$$

$$B^{\bullet -} + e^- \rightleftharpoons B^{2-} \; E^\circ_{2B}, \qquad k_{s,2B}, \alpha_{2B} \tag{5}$$

Reactions 1 and 2 constitute the CE sequence leading to the plateau between −1.0 and −1.6 V. Reaction 3 accounts for the main reduction peak at −1.7 V for which there is no associated oxidation peak owing to the occurrence of rapid reaction 4. Finally, on the return sweep, a large anodic peak is seen for oxidation of $B^{\bullet -}$ near −1.0 V (reverse of reaction 2) that is followed by the conversion of electrogenerated B to A (reverse of reaction 1). The second step of reduction of the B form (reaction 5) was not required in the simulation shown in Figure 3 as the sweep did not encompass potentials in which that reaction occurs (cf. Figure 2). Voltammograms were obtained for eleven scan rates from 0.1 to 30 V/s and the simulation parameters that gave the best average fit are summarized in Table 2. This means that adjustments in these parameters might lead to improved fits for any given scan rate (e.g., Figure 3) but we prefer to find the set of parameters that gives the best average agreement. The only parameter that was not adjusted was $K_{A\rightleftharpoons B}$, which was maintained at the value that was determined in a separate experiment (see above).

An increase in temperature will cause a small increase in $K_{A\rightleftharpoons B}$ and more importantly will cause increases in $k_{A\to B}$ and $k_{B\to A}$. The result of these changes is that the kinetic plateau current increases in magnitude at the expense of the major reduction peak (Figure 4). Again, a set of simulation parameters was found that provided the best average fit of simulation to experiment for a range of scan rates at 82 °C. These parameters are listed in Table 2 along with those for five other temperatures. Examples of the comparison of simulated and experimental voltammograms are provided in the Supporting Information.

The electrochemical parameters include standard potentials, E°_{1B} and E°_{1A}, that move 35−40 mV in the negative direction on increasing the temperature from 25 to 82 °C and rate constants, $k_{s,1B}$ and $k_{s,1A}$, that increase smoothly with increasing temperature. As mentioned above, the equilibrium constant $K_{A\rightleftharpoons B}$ was not allowed to vary during optimization but was maintained at the values measured in the spectrophotometric measurement described earlier. The rate constants, $k_{A\to B}$ and $k_{B\to A}$, increase with increasing temperature. The equilibrium constant, $K_{A-\rightleftharpoons B-}$, is not adjustable with its value being defined by the entered values of E°_{1B}, E°_{1A}, and $K_{A\rightleftharpoons B}$. Its value, 1.6×10^{11} at 25 °C, corresponds to $\Delta G^\circ_{A-\rightleftharpoons B-} = -15.3$ kcal/mol, which is consistent with the calculated gas-phase free energy difference, −17.2 kcal/mol (Table 1). Large values for the rate constant of isomerization of the anion radical, $k_{A-\to B-}$, were obtained, but their magnitude is uncertain because we were unable to detect the transient A form of the anion radical and thus get a firm value of the rate constant.

We also confirmed by simulation (not shown) that the values of E°_{1B} and the rate constants, $k_{A\to B}$ and $k_{B\to A}$, reported in Table 2 gave good fits to the $B + e^- \rightleftharpoons B^{\bullet -}$ reduction peak in two-cycle experiments such as that shown in Figure 2.

3.3 Voltammetric Study of 7. As seen in Figure 5, the behavior of **7** resembles that of **6** (Figure 2) except that the two reduction peaks are closer together owing to similar values of E°_{1A} and E°_{2B}. Also, the CE current due to reactions 1 and 2 is undetectable in Figure 5 because the equilibrium constant, $K_{A\rightleftharpoons B}$, is extremely small, and the rate constants, $k_{A\to B}$ and $k_{B\to A}$, are not large enough to provide a detectable current. Nevertheless, the voltammograms can be fit by the same mechanism used for **6** (Scheme 3; reactions 1−4) except that the second reduction of B, $B^{\bullet -} + e^- \rightleftharpoons B^{2-}$ (reaction 5), must be included due to the closeness of the two reduction peaks. At higher scan rates, the two peaks merge because of a negative shift of the first related to the small value of $k_{s,1A}$. It also was necessary to include a solution-phase electron-transfer reaction, $A^{\bullet -} + B^{\bullet -} \rightleftharpoons A + B^{2-}$, occurring with large rate constants, to simulate the data satisfactorily. This reaction accounted for the rather abrupt plunge of the current to zero after passing through the peak for oxidation of B^{2-} (Figure 5).

Figure 6 shows that at an elevated temperature the CE plateau is detectable because of increases in $K_{A\rightleftharpoons B}$, $k_{A\to B}$, and $k_{B\to A}$. Data for seven temperatures from 25 to 82 °C were matched by simulation, and the parameters that provided the best average fit for each temperature are listed in Table 3. Other examples

TABLE 2: Experimental Conditions and Simulation Parameters for Xanthylideneanthrone, 6[a]

Electrochemical Reactions

temp/°C	$E°_{1B}$/V	$E°_{1A}$/V	$k_{s,1B}$/cm s^{-1}	$k_{s,1A}$/cm s^{-1}	α_{1B}	α_{1A}	10^6D/cm^{2}s^{-1}
25.0	−0.979	−1.780	0.067	0.089	0.50	0.52	5.30
35.0	−0.982	−1.786	0.075	0.094	0.50	0.52	6.47
45.0	−0.987	−1.793	0.081	0.143	0.50	0.52	7.00
55.0	−0.992	−1.796	0.086	0.200	0.50	0.52	8.04
64.5	−0.997	−1.799	0.121	0.200	0.50	0.52	9.57
74.0	−1.004	−1.804	0.145	0.220	0.50	0.52	10.8
82.0	−1.018	−1.815	0.209	0.270	0.50	0.52	12.0

Chemical Reactions

temp/°C	$K_{A\rightleftharpoons B}$	$k_{A\rightarrow B}$/s^{-1}	$k_{B\rightarrow A}$/s^{-1}	$K_{A-\rightleftharpoons B-}$	$k_{A-\rightarrow B-}$/s^{-1}	$k_{B-\rightarrow A-}$/s^{-1}	range
25.0	4.8×10^{-3}	0.44	91	1.6×10^{11}	1.0×10^{4}	6.1×10^{-8}	0.1−30.0
35.0	5.5×10^{-3}	1.0	1.9×10^{2}	7.9×10^{10}	3.6×10^{4}	4.5×10^{-7}	0.2−30.0
45.0	7.0×10^{-3}	1.9	2.8×10^{2}	4.2×10^{10}	7.7×10^{4}	1.8×10^{-6}	0.5−30.0
55.0	7.6×10^{-3}	4.2	5.5×10^{2}	1.7×10^{10}	8.9×10^{4}	5.3×10^{-6}	0.5−30.0
64.5	8.8×10^{-3}	7.1	8.1×10^{2}	8.2×10^{9}	2.0×10^{5}	2.4×10^{-5}	1.0−30.0
74.0	1.0×10^{-2}	14	1.4×10^{3}	4.1×10^{9}	2.8×10^{5}	6.7×10^{-5}	1.0−30.0
82.0	1.1×10^{-2}	26	2.4×10^{3}	2.2×10^{9}	5.9×10^{5}	2.7×10^{-4}	1.0−30.0

[a] The same values were used to fit all scan rates in the range (final column) at each temperature. Potentials are with respect to the ferrocene couple measured in DMF at each temperature. Resistance compensation. Format: temperature (°C)/total resistance (Ω)/resistance electronically compensated (Ω); 25/290/250; 35/260/250; 45/235/220; 55/220/220; 64.5/190/180; 74/185/160; 82/175/140. The residual uncompensated resistance was included in the simulations. Diffusion coefficients of all species were set equal to the number shown. Solutions were prepared at 25 °C. Concentrations at other temperatures have not been corrected for thermal expansion.

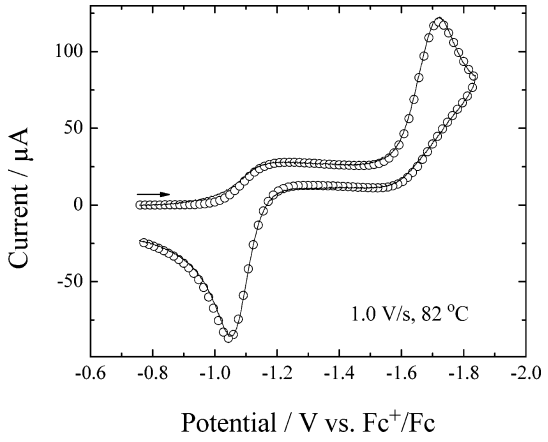

Figure 4. Voltammogram (solid curve) of 2.40 mM xanthylideneanthrone, **6**. Symbols: simulation using the parameter values listed in Table 2.

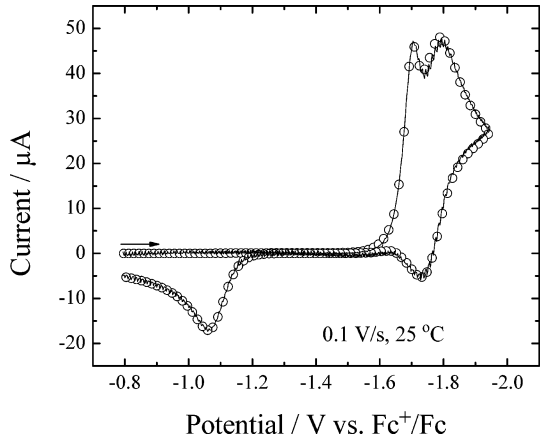

Figure 5. Voltammogram (solid curve) of 2.00 mM thioxanthylideneanthrone, **7**. Symbols: simulation using the parameter values listed in Table 3.

of the comparison of simulation and experiment are provided in the Supporting Information.

In this case, it was not possible to evaluate $K_{A\rightleftharpoons B}$ in the manner used for **6** because **7** is not thermochromic. For this

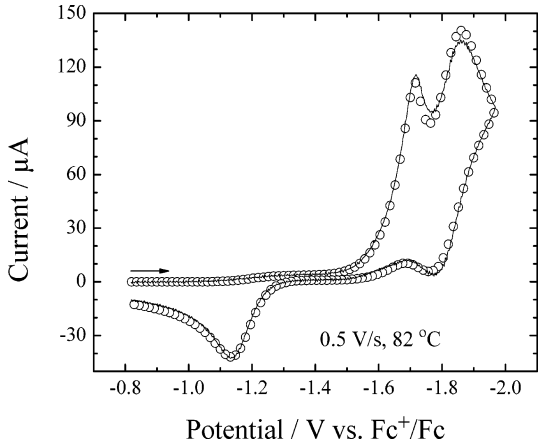

Figure 6. Voltammogram (solid curve) of 2.00 mM thioxanthylideneanthrone, **7**. Symbols: simulation using the parameter values listed in Table 3.

reason, we used calculated values of $K_{A\rightleftharpoons B}$ based on the gas-phase free energy change, 9.2 kcal/mol, as inputs in the simulation program. As can be seen in Table 3, the equilibrium constants are small and in the range of 10^{-7} to 10^{-6}, which is consistent with the inability to detect the colored B form in the available range of temperatures. Again, when the temperature is increased, the rate constants, $k_{A\rightarrow B}$ and $k_{B\rightarrow A}$, increase so that a small kinetic CE plateau is detected (Figure 6). The best-fit simulation parameters (Table 3), indicate that $k_{A\rightarrow B}$ increases substantially with increases in temperature, but $k_{B\rightarrow A}$ is large and approximately independent of temperature, which is consistent with a reaction with a very low activation energy. The large values of $k_{B\rightarrow A}$ are consistent with the fact that two-cycle experiments, like those in Figure 2, do not show a peak for B + $e^- \rightleftharpoons B^{\bullet-}$ even at 100 V/s and −16 °C.

Again, the B form of the anion radical is strongly favored, and the corresponding equilibrium constant is large and is dictated by the entered values of $K_{A\rightleftharpoons B}$, $E°_{1A}$, and $E°_{1B}$. The corresponding free energy change at 25 °C, $\Delta G°_{A-\rightleftharpoons B-}$, is −9.5 kcal/mol compared to the calculated gas-phase value of −11.0 kcal/mol (Table 1). As with compound **6**, fast scan rates and low temperatures do not allow detection of a peak for oxidation

TABLE 3: Experimental Conditions and Simulation Parameters for Thioxanthylideneanthrone, 7[a]

Electrochemical Reactions

temp/°C	$E°_{1B}$/V	$E°_{1A}$/V	$E°_{2B}$/V	$k_{s,1B}$/cm s^{-1}	$k_{s,1A}$/cm s^{-1}	$k_{s,2B}$/cm s^{-1}	10^6D/cm^{2}s^{-1}
25.0	−0.923	−1.736	−1.769	0.230	0.010	0.120	5.06
35.0	−0.928	−1.740	−1.770	0.280	0.012	0.140	5.69
45.0	−0.938	−1.747	−1.779	0.300	0.020	0.110	6.65
55.0	−0.946	−1.750	−1.787	0.370	0.028	0.120	7.58
64.5	−0.960	−1.753	−1.796	0.350	0.032	0.100	8.63
74.0	−0.976	−1.758	−1.808	0.330	0.034	0.140	9.66
82.0	−0.991	−1.770	−1.821	0.420	0.036	0.140	11.20

Chemical Reactions

temp/°C	$K_{A\rightleftharpoons B}$	$k_{A\rightarrow B}$/s^{-1}	$k_{B\rightarrow A}$/s^{-1}	$K_{A-\rightleftharpoons B-}$	$k_{A-\rightarrow B-}$/s^{-1}	$k_{B-\rightarrow A-}$/s^{-1}	range
25.0	1.8×10^{-7}	67	3.7×10^{8}	9.9×10^{6}	8.4×10^{2}	5.9×10^{-6}	0.1−30.0
35.0	3.0×10^{-7}	1.4×10^{2}	4.8×10^{8}	5.8×10^{6}	1.4×10^{3}	1.6×10^{-6}	0.2−30.0
45.0	4.8×10^{-7}	2.3×10^{2}	4.8×10^{8}	3.2×10^{6}	2.8×10^{3}	5.3×10^{-6}	0.2−30.0
55.0	7.5×10^{-7}	5.1×10^{2}	6.8×10^{8}	1.7×10^{6}	5.6×10^{3}	1.9×10^{-4}	0.3−30.0
64.5	1.1×10^{-6}	1.2×10^{3}	1.1×10^{9}	7.6×10^{5}	1.0×10^{4}	5.7×10^{-4}	0.3−30.0
74.0	1.6×10^{-6}	1.4×10^{3}	8.4×10^{8}	3.6×10^{5}	2.7×10^{4}	3.9×10^{-3}	0.5−30.0
82.0	2.2×10^{-6}	2.7×10^{3}	1.2×10^{9}	2.5×10^{5}	2.2×10^{5}	5.1×10^{-2}	0.5−30.0

[a] The same values were used to fit all scan rates in the range (final column) at each temperature. Potentials are with respect to the ferrocene couple measured in DMF at each temperature. Resistance compensation. Format: temperature (°C)/total resistance (Ω)/resistance electronically compensated (Ω); 25/290/250; 35/260/250; 45/235/220; 55/220/220; 64.5/190/180; 74/185/160; 82/175/140. The residual uncompensated resistance was included in the simulations. Diffusion coefficients of all species were set equal to the number shown. Solutions were prepared at 25 °C. Concentrations at other temperatures have not been corrected for thermal expansion. $\alpha_{1A} = \alpha_{1B} = \alpha_{2B} = 0.50$. The disproportionation reaction of the two anion radicals, $A^{\bullet-} + B^{\bullet-} \rightleftharpoons A + B^{2-}$, was also included in the simulation, where the equilibrium constants were dictated by the values of the standard potentials $E°_{1A}$ and $E°_{2B}$ and the rate constants were made large. A small irreversible first-order loss of B^{2-} ($k_f = 0.38$ s^{-1} at 25 °C) was also included in the simulations.

of $A^{\bullet-}$ indicating that the reaction is very fast, which is consistent with the simulation parameters (Table 3).

The first step of reduction of **6** and **7** is a one-electron reduction that occurs in two steps: reaction 3 (electron transfer) followed by reaction 4 (structural change). At higher temperatures, there is an intervention to a certain extent of reaction 1 (structural change) followed by reaction 2 (electron transfer). For either pathway, it is clear that these are two-step reactions because intermediate species are detected. The reaction proceeds in the forward direction by the sequence $A \rightarrow A^{\bullet-} \rightarrow B^{\bullet-}$ and in the reverse direction by $B^{\bullet-} \rightarrow B \rightarrow A$. That is, we can say with some certainty that the reduction of A to $B^{\bullet-}$ cannot be a single-step process with concerted electron transfer and structural change, $A + e^- \rightleftharpoons B^{\bullet-}$. However, for the one-electron reduction of **8** this distinction is not so clear. Nevertheless, we will present evidence that the reaction proceeds by two-step processes rather than a one-step concerted process.

3.4 Voltammetric Study of 8. As discussed earlier, **8** undergoes a structural change upon reduction that is quite analogous to that of **6** and **7**. Specifically, the neutral form of **8** features a folded anthrone unit with the diphenylmethylene system only slightly twisted with respect to the anthrone (Table 1). However, the anion radical of **8** has a planar anthrone system and the diphenylmethylene system is strongly twisted, 54° by calculation (Scheme 2) and 90° as inferred from EPR data.

Voltammograms of **8** are shown in Figure 7. There are two reduction steps, each of which is relatively reversible. However, some reaction of the highly basic B^{2-} with proton sources in the medium is seen, a product of which produces a small oxidation peak near −0.7 V. This peak is not seen when the scan encompasses only the first step of reduction (Figure 7).

In fact, the first set of peaks would appear to be due to a simple quasireversible process, $A + e^- \rightleftharpoons B^{\bullet-}$ (diagonal reaction in Scheme 3). Though not obvious in Figure 7, an increase in peak separation is clearly seen at faster scan rates. This quasireversibility might be attributed to a significant inner reorganization energy due to the structural change associated

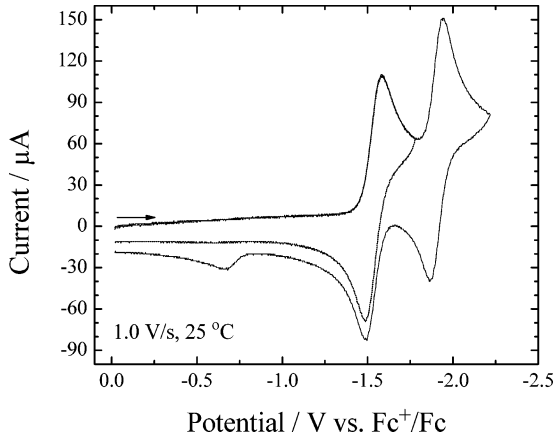

Figure 7. Voltammograms of 2.17 mM 10-(diphenylmethylene)-anthrone, **8**. Backgrounds have not been subtracted.

with the reaction. Initially, we attempted to fit the voltammograms with the simple one-step mechanism. This implies that electron transfer and structural change are concerted, using the Butler−Volmer formulation of electron-transfer kinetics with the adjustable parameters being $E°_{1AB}$, $k_{s,1AB}$, and α_{1AB}. Fitting of the voltammograms was not satisfactory, particularly at lower temperatures and/or larger scan rates. An example is shown in Figure 8A, where the simulation is based on the parameter values that provided the best average fit for eleven scan rates from 0.1 to 30 V/s obtained at −8 °C. As mentioned above, the fit is considerably better at low scan rates in which the voltammogram is close-to-reversible in shape and in which any model of electron-transfer kinetics will tend to give the same result. Clearly, the Butler−Volmer model fails to account for the detailed shape of the voltammogram in Figure 8A. We are confident that the deviations are not due to improper correction for solution resistance as the total uncompensated resistance was carefully determined at each temperature by studies of ferrocene as reported earlier.[8] Part of this resistance was compensated electronically and the remainder was included in the simulations.

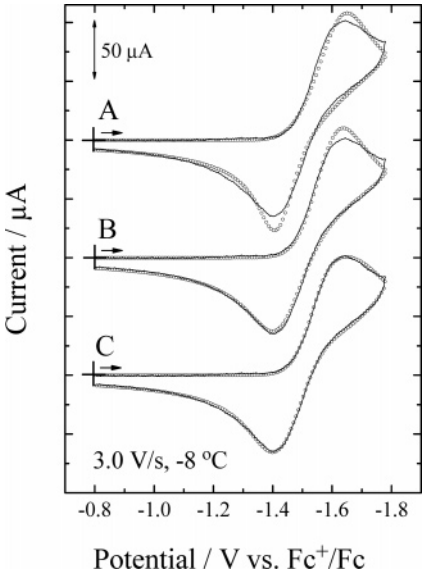

Figure 8. Voltammogram (solid curve) of 2.17 mM 10-(diphenylmethylene)anthrone, **8**. Simulations (symbols): A: Butler−Volmer formulation of electron-transfer kinetics. $E°_{1AB} = -1.506$ V, $k_{s,1AB} = 0.0023$ cm/s, $\alpha_{1AB} = 0.39$. B: Marcus formulation with α_{1AB} from eq 6 with parameters listed in Table 4. C: Square Scheme 3 with parameters listed in Table 5.

TABLE 4: Experimental Conditions and Simulation Parameters for 10-(diphenylmethylene)Anthrone, 8. Simulation Model: Potential-Dependent Alpha According to Eq 6[a]

temp/°C	$E°_{1AB}$/V	$k_{s,1AB}$/cm s^{-1}	λ/eV	10^6D/cm^{2}s^{-1}
25.0	−1.533	0.0128	0.21	5.31
18.0	−1.532	0.0088	0.21	4.95
10.0	−1.524	0.0053	0.21	4.59
2.0	−1.520	0.0041	0.25	3.99
−8.0	−1.511	0.0026	0.27	3.32

[a] The same values were used to fit all scan rates from 0.1 to 30 V/s at a given temperature. Potentials are with respect to the ferrocene couple measured in DMF at each temperature. Resistance compensation. Format: temperature (°C)/total resistance (Ω)/resistance electronically compensated (Ω); 25/290/250; 18/320/280; 10/340/300; 2/380/340; −8/470/430. The residual uncompensated resistance was included in the simulations. Diffusion coefficients of all species were set equal to the number shown. Solutions were prepared at 25 °C. Concentrations at other temperatures have not been corrected for thermal contraction.

A model that will give broadened peaks for both the cathodic and anodic process is that of Marcus.[20] Here, the electron-transfer coefficient, α_{1AB}, is not constant but varies with potential according to eq 6 in which λ is the total reorganization energy.

$$\alpha_{1AB} = \frac{1}{2} + \frac{F(E - E^o_{1AB})}{2\lambda} \qquad (6)$$

In Figure 8B, a simulation is compared to the same experimental curve in A. Again, the simulation parameters are those that provide the best average fit for the eleven scan rates from 0.1 to 30 V/s. The fit is somewhat better particularly in the region of the anodic peak, but the shape of the cathodic peak does not match experiment. The parameters could be adjusted to provide a somewhat better fit for the scan rate used in Figure 8B, but these parameters would bring about worse agreement at the other scan rates. The simulation parameters used for the Marcus model are listed in Table 4.

In addition to the fact that the fits of simulation to experiment are not satisfactory, there is another reason to reject this model. The optimized reorganization energies, λ, which range from 0.21 to 0.27 eV, are unreasonably small. For example, the reorganization energies evaluated for a series of aromatic compounds in DMF fall in the range of 0.5 to 0.8 eV, mainly reflecting the outer reorganization energy.[21] There is no apparent reason that the reorganization energy for **8** should be one-half or less of that for other similar compounds.

We next turned to the same mechanism successfully used for **6** and **7**, namely, the square Scheme 3. This was not an obvious choice as the voltammograms of **8** differ significantly from those of **6** and **7**, particularly because the oxidation peak for **8** is very close to the reduction peak, which is not located at the much less negative potentials as is the oxidation peak of $B^{\bullet-}$ for **6** and **7**. However, by adjusting $E°_{1B}$ so that it was close to $E°_{1A}$ and choosing $K_{A\rightleftharpoons B}$ to be not as small as for **6** and **7**, it was possible to obtain much improved fits (Figure 8C). Again, the parameter values used in Figure 8C are those that provided the best average fit for the voltammograms obtained from 0.1 to 30 V/s. Data for other temperatures were also simulated, and the simulation parameters are summarized in Table 5. Other examples of the comparison of simulation and experiment are provided in the Supporting Information.

Examination of Table 5 shows that the optimized value of $E°_{1B}$ is only 160 mV positive of $E°_{1A}$, and $K_{A-\rightleftharpoons B-}$ is not extremely large (58 at 25 °C). Consequently, $K_{A\rightleftharpoons B}$ is fairly sizable, 0.12 at 25 °C (1.2 kcal/mol). Though by DFT calculations we could not identify a B form for neutral **8**, one B-like structure was found by single-point calculations to be only 2 kcal/mol more energetic than the A form, so $K_{A\rightleftharpoons B} = 0.12$ seems reasonable. The electron-transfer reactions were treated according to the Butler−Volmer formulation, and the values of α_{1A} and α_{1B}, 0.42 and 0.57, respectively, fall in the normal range.

The danger in applying the two-step mechanism embodied in the square Scheme 3 as compared to the single-step reaction according to the Butler−Volmer or Marcus formulation of the electron-transfer reactions is that the abundance of adjustable parameters in the two-step mechanism might allow multiple sets of simulation parameter values to provide equally good agreement between simulation and experiment, that is, there may not be a unique set of simulation parameter values. Several attempts were made to move one or more parameters from their optimized values and repeat the fitting. In each case, the optimization returned the parameters to values close to the original ones. Nevertheless, we cannot be certain that we have found a global minimum or that the parameter values, which are chemically reasonable, are close to the real values.

Nevertheless, we will assume that the best-fit parameter values are realistic and demonstrate why the square scheme can give the much improved fits that were found. Figure 9 repeats the simulation shown in Figure 8C using a special version of DigiElch that allows the total current (solid) to be divided into two components: components arising from the reaction $A + e^- \rightleftharpoons A^{\bullet-}$ (A-current; dashed) and components from the reaction $B + e^- \rightleftharpoons B^{\bullet-}$ (B-current; dotted). The result is unexpected. The optimization in the simulation program led to parameter values that cause most of the current near the foot of the reduction peak to proceed as a CE process, $A \rightarrow B$; $B + e^- \rightarrow B^{\bullet-}$ (B-current). At more negative potentials, closer to $E°_{1A}$, the A-current increases but does not surpass the B component until the potential is close to the cathodic peak. The continued growth of the A-current past the peak potential is what allows the simulation to match the slow decay in current that is seen, something that neither the Butler−Volmer nor the Marcus treatment is able to achieve (Figure 8A and 8B).

TABLE 5: Experimental Conditions and Simulation Parameters for 10-(diphenylmethylene)Anthrone, 8. Simulation Model: Square Scheme 3[a]

Electrochemical Reactions

temp/°C	$E°_{1B}$/V	$E°_{1A}$/V	$k_{s,1B}$/cm s^{-1}	$k_{s,1A}$/cm s^{-1}	α_{1B}	α_{1A}	$10^6 D$/cm^{2}s^{-1}
25.0	−1.475	−1.635	0.037	0.017	0.57	0.42	5.33
18.0	−1.472	−1.628	0.025	0.011	0.57	0.42	4.85
10.0	−1.464	−1.613	0.017	0.005	0.57	0.42	4.59
2.0	−1.454	−1.602	0.014	0.004	0.57	0.42	4.04
−8.0	−1.442	−1.578	0.010	0.004	0.57	0.39	3.29

chemical reactions

temp/°C	$K_{A\rightleftharpoons B}$	$k_{A\rightarrow B}$/s^{-1}	$k_{B\rightarrow A}$/s^{-1}	$K_{A-\rightleftharpoons B-}$	$k_{A-\rightarrow B-}$/s^{-1}	$k_{B-\rightarrow A-}$/s^{-1}	range
25.0	0.12	6.0×10^3	5.2×10^4	58	2.0×10^4	3.5×10^2	0.1−30.0
18.0	0.10	4.4×10^3	4.5×10^4	52	1.5×10^4	2.9×10^2	0.1−30.0
10.0	0.09	3.0×10^3	3.4×10^4	40	7.7×10^3	1.9×10^2	0.1−30.0
2.0	0.06	1.4×10^3	2.1×10^4	33	3.8×10^3	1.1×10^2	0.1−30.0
−8.0	0.05	5.5×10^2	1.1×10^4	20	1.3×10^3	64	0.1−30.0

[a] See footnote to Table 4.

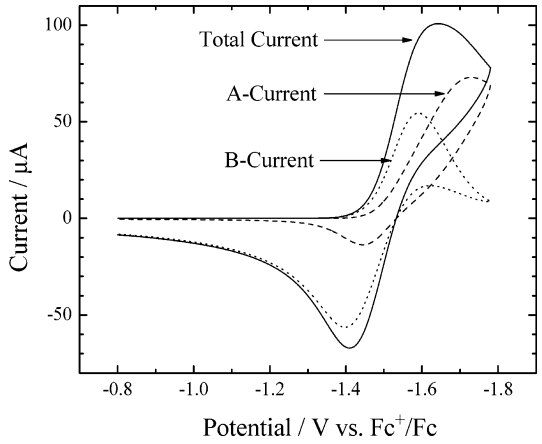

Figure 9. Simulation identical to that in Figure 8C except that the total current has been divided into two components, one for $A + e^- \rightleftharpoons A^{\bullet -}$ (A-current) and the other for $B + e^- \rightleftharpoons B^{\bullet -}$ (B-current).

3.5 Voltammetric Study of 9. As discussed in Section 3.1, the formation of the A forms for **6**−**8** is facilitated by the folding of the anthrone unit in which folding is in turn made possible by the six-membered ring having a carbonyl group. This bridge is absent in the fluorene system making it impossible to form a folded A form for **9**. Consequently, all three species, the neutral, anion radical, and dianion of **9** have planar fluorene groups and are twisted B-like structures with the degree of twisting increasing in that order.

Consistent with these structures, the voltammetry of **9** shows two steps of reduction, $B + e^- \rightleftharpoons B^{\bullet -}$ and $B^{\bullet -} + e^- \rightleftharpoons B^{2-}$, with B^{2-} being lost rapidly even under the driest conditions. However, at rapid scan rates at 25 °C, oxidation of B^{2-} can be detected, and simulation of the voltammograms gives −2.021 and −2.372 V for $E°_{1B}$ and $E°_{2B}$, respectively.

4. Conclusion

This work demonstrates the strong relationship between structure and electron-transfer reactivity for a group of unsymmetrical crowded ethylenes. Compounds **6**−**8** contain an anthrone moiety that folds in response to steric interaction with the group attached to the 10 position (A form). In **6** and **7**, this group, xanthylidene and thioxanthylidene, respectively, also is folded. Upon reduction, the anion radicals undergo twisting of the 10 substituent with respect to the anthrone moiety (B form). The twisted B forms are better electron acceptors than the folded A forms. For compound **6**, the B form is thermally accessible, and the equilibrium constant for conversion of A to B was evaluated. The first step of reduction of **6** and **7** follows a square scheme, and voltammetry allowed the evaluation of thermodynamic and kinetic parameters over a range of temperatures. The reduction of **8** also appears to follow the square scheme but the conclusion is not as firm as with the other two anthrones as one-step mechanisms involving concerted electron transfer and structural change provide fits to the data, though not as good as with the square scheme.

Acknowledgment. This research was supported by the National Science Foundation, Grant CHE 0347471. We thank Dr. Manfred Rudolph, Friedrich-Schiller-University Jena, Jena, DE for providing the special version of DigiElch used to generate the simulations shown in Figure 9.

Supporting Information Available: Examples of fits of simulations to the experimental voltammograms of **6**−**8**. This material is available free of charge via the Internet at http://pubs.acs.org.

References and Notes

(1) Evans, D. H.; O'Connell, K. M. In *Electroanalytical Chemistry*; Bard, A. J., Ed.; Dekker: New York, 1986; Vol. 14, pp 143−154.

(2) (a) Hu, K.; Evans, D. H. *J. Electroanal. Chem.* **1997**, *423*, 29−35. (b) Gruhn, N. E.; Macías-Ruvalcaba, N. A.; Evans, D. H. *J. Phys. Chem. A* **2006**, *110*, 5650−5655.

(3) Gruhn, N. E.; Macías-Ruvalcaba, N. A.; Evans, D. H. *Langmuir*, [Online early access]. DOI: 10.1021/la0611460. Published online: June 30, 2006. http://pubs.acs.org/cgi-bin/asap.cgi/langd5/asap/html/la0611460.html.

(4) Kraiya, C.; Evans, D. H. *J. Electroanal. Chem.* **2004**, *565*, 29−35.

(5) Macías-Ruvalcaba, N. A.; Evans, D. H. *J. Phys. Chem. B* **2006**, *110*, 5155−5160.

(6) Lehmann, M. W.; Singh, P.; Evans, D. H. *J. Electroanal. Chem.* **2003**, *549*, 137−143.

(7) Hu, K.; Evans, D. H. *J. Phys. Chem.* **1996**, *100*, 3030−3036.

(8) Macías-Ruvalcaba, N. A.; Evans, D. H. *J. Phys. Chem.* **2005**, *109*, 14642−14647.

(9) Schönberg, A.; Ismail, A. F. A.; Asker, W. *J. Chem. Soc.* **1946**, 442−446.

(10) (a) Padova, M. R. *Compt. Rend.* **1906**, *143*, 121−123. (b) Le Fèvre, R. J. W.; Youhotsky, I. *J. Chem. Soc.* **1953**, 1318−1319.

(11) Kortüm, G.; Zoller, W. *Chem. Ber.* **1970**, *103*, 2062−2076.

(12) (a) Rudolph, M. *J. Electroanal. Chem.* **2003**, *543*, 23−29. (b) Rudolph, M. *J. Electroanal. Chem.* **2004**, *571*, 289−307. (c) Rudolph, M. *J. Electroanal. Chem.* **2003**, *558*, 171−176. (d) Rudolph, M. *J. Comput. Chem.* **2005**, *26*, 619−632. (e) Rudolph, M. *J. Comput. Chem.* **2005**, *26*, 633−641. (f) Rudolph, M. *J. Comput. Chem.* **2005**, *26*, 1193−1204.

(13) Frisch, M. J.; Trucks, G. W.; Schlegel, H. B.; Scuseria, G. E.; Robb, M. A.; Cheeseman, J. R.; Montgomery, Jr., J. A.; Vreven, T.; Kudin, K. N.; Burant, J. C.; Millam, J. M.; Iyengar, S. S.; Tomasi, J.; Barone, V.; Mennucci, B.; Cossi, M.; Scalmani, G.; Rega, N.; Petersson, G. A.; Nakatsuji, H.; Hada, M.; Ehara, M.; Toyota, K.; Fukuda, R.; Hasegawa, J.; Ishida, M.; Nakajima, T.; Honda, Y.; Kitao, O.; Nakai, H.; Klene, M.; Li, X.; Knox, J. E.; Hratchian, H. P.; Cross, J. B.; Adamo, C.; Jaramillo, J.;

Gomperts, R.; Stratmann, R. E.; Yazyev, O.; Austin, A. J.; Cammi, R.; Pomelli, C.; Ochterski, J. W.; Ayala, P. Y.; Morokuma, K.; Voth, G. A.; Salvador, P.; Dannenberg, J. J.; Zakrzewski, V. G.; Dapprich, S.; Daniels, A. D.; Strain, M. C.; Farkas, O.; Malick, D. K.; Rabuck, A. D.; Raghavachari, K.; Foresman, J. B.; Ortiz, J. V.; Cui, Q.; Baboul, A. G.; Clifford, S.; Cioslowski, J.; Stefanov, B. B.; Liu, G.; Liashenko, A.; Piskorz, P.; Komaromi, I.; Martin, R. L.; Fox, D. J.; Keith, T.; Al-Laham, M. A.; Peng, C. Y.; Nanayakkara, A.; Challacombe, M.; Gill, P. M. W.; Johnson, B.; Chen, W.; Wong, M. W.; C. Gonzalez, C.; Pople, J. A. *Gaussian 03*, Revision B.05; Gaussian, Inc.: Pittsburgh, PA, 2003.

(14) Hirshberg, Y.; Fischer, E. *J. Chem. Soc.* **1953**, 629−636.

(15) Biedermann, P. U.; Stezowski, J. J.; Agranat, I. *Chem. Comm.* **2001**, 954−955.

(16) Kazama, S.; Sato, E.; Kamiya, M.; Akahori, Y. *Chem. Pharm. Bull.* **1980**, *28*, 2216−2220.

(17) Luisa, M.; Franco, T. M. B.; Herold, B. J.; Evans, J. C.; Rowlands, C. C. *J. Chem. Soc., Perkin Trans. 2* **1988**, 443−449.

(18) (a) The C−O−C and C−S−C angles are 112° and 99.05° in dimethyl ether and dimethyl sulfide, respectively.[18b] (b) *CRC Handbook of Chemistry and Physics*, 82nd Ed.; Lide, D. R., Ed.; CRC Press: Boca Raton, FL, 2001; p 9−33.

(19) Grubb, W. T.; Kistiakowsky, G. B. *J. Am. Chem. Soc.* **1950**, *72*, 419−424.

(20) Bard, A. J.; Faulkner, L. R. *Electrochemical Methods. Fundamentals and Applications*, 2nd Ed.; Wiley: New York, 2001; pp 117−123.

(21) Kojima, H.; Bard, A. J. *J. Am. Chem. Soc.* **1975**, *97*, 6317−6324.